Thermodynamic Studies of 10-Hydroxy-camptothecin in Aqueous Solutions

Sasank Kunadharaju and Michalakis Savva*

Division of Pharmaceutical Sciences, Arnold & Marie Schwartz College of Pharmacy & Health Sciences, Long Island University, Brooklyn, New York 11201

Physicochemical characterization of 10-hydroxy-camptothecin (10-HC) was carried out to fully characterize the poor aqueous solubility and hydrolytic instability that severely limit its efficient delivery and pharmacological activity. Molecular and system properties were determined from titration, partition, and solubility studies using UV and fluorescence spectroscopy, while solid state characterization of the 10-HC was carried out with X-ray, DSC, and TGA. The enthalpies of solution of the unionized and ionized forms of 10-HC, as deduced from isothermal and iso-pH equilibrium solubility measurements, were 45.4 kJ·mol^{-1} and 22.7 kJ·mol^{-1}, respectively. The pK_a of 10-HC was determined to be 1.42 at 25 °C, while the basicity of the quinoline group of 10-HC was shown to decrease with increasing temperature due to a positive enthalpy of deprotonation of 23.6 kJ·mol^{-1}. The intrinsic partition coefficient of 10-HC was determined to be 6.49, which is significantly smaller than that of the parent camptothecin. Evidently, the hydroxyl substitution on the A ring of camptothecin renders the molecule considerably more polar, though still hydrophobic and sparingly soluble in aqueous media. Dissolution studies supported by X-ray and thermal analysis revealed polymorphism and serious metastability of the 10-HC anhydrous form in aqueous solutions. The aqueous solubility of 10-HC-lactone monohydrate was found to be pH and temperature dependent with an estimated intrinsic solubility of (1.81 ± 0.2) μM. Contrary to the low intrinsic solubility, the solubility of 10-HC in extremely acidic media increased by more than 3 orders of magnitude. This feature can be used to facilitate fabrication of highly efficient drug delivery systems for 10-HC systemic administration.

Introduction

The pentacyclic alkaloid, 10-hydroxy-camptothecin (10-HC; Scheme 1), isolated from the Chinese tree, *Camptotheca acuminata*, inhibits the activity of topoisomerase I and has a broad spectrum of anticancer activity in vitro and in vivo.[1] Nonetheless, the efficient delivery of this drug is extremely challenging because of its poor water solubility and the facile conversion of the active lactone form into the hydrolyzed product (Scheme 2) at physiological conditions.[2−5] More specifically, the α-hydroxy δ-lactone moiety undergoes reversible hydrolysis at and above pH 5, to a ring-opened carboxylate form, which is up to 10 times less potent compared to the native lactone form.[4,6] Moreover, polarity and other differences between the two chemical species promote their differential interaction with endogenous proteins that further perturbs their in vivo equilibrium and consequently affects the transport and pharmacological activity of the drug.[7] Several investigators have proposed formulation strategies to circumvent the problems associated with the stability of 10-HC, but detailed molecular characterization is lacking in the literature.[8−11] Most of the formulations that had some success were based on a single strategy of encapsulating the drug into a hydrophobic vehicle, aiming to increase loading and stability of camptothecin analogues. In our view, novel formulation strategies for optimum delivery of 10-HC can only surface upon detailed physicochemical characterization of the drug.

In this regard, thermodynamic studies of 10-HC in aqueous solutions, including pK_a, and effect of pH and temperature on the solubility were conducted to obtain estimates of the intrinsic solubility of 10-HC and saturated concentration of the corresponding hydrochloride salt. To gain more insight into issues of oral absorption, solid state characterization, diffusivity and partition coefficients were evaluated for both the ionized and unionized form of the drug.

Scheme 1. Structure 20-(*S*)-10-Hydroxy-camptothecin

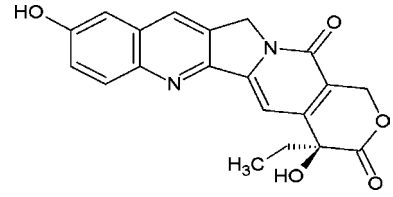

Scheme 2. Reversible Hydrolysis Reaction of 10-HC-Lactone ($C_{20}H_{16}N_2O_5$) to 10-HC-Carboxylate ($C_{20}H_{17}N_2O_6$)

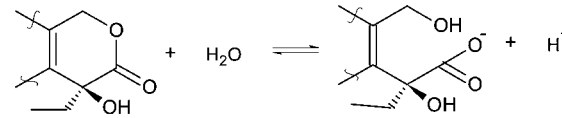

10-HC-lactone 10-HC-carboxylate

Materials and Experimental Methods

Materials. The 20-(*S*) isomer of 10-HC (4-ethyl-4,9-dihydroxy-1*H*-pyrano(3′,4′:6,7)indolizino(1,2-b)quinoline-3,14 (4*H*,12*H*)-dione, CASRN: 19685-09-7, $C_{20}H_{16}N_2O_5$, 364.351 g·mol^{-1}, stated mass fraction purity > 98 %) was purchased from Dayang Chemicals, China. In close agreement with the vendor's stated purity, elemental analysis of the 10-HC-lactone carried out by

* Corresponding author. Tel.: +1-718-488-1471. Fax: +1-718-780-4586. E-mail: msavva@liu.edu.

10.1021/je900283v CCC: $40.75
Published on Web 06/25/2009

Robertson Microlit Laboratories (Madison, NJ) yielded a mass fraction purity of 96 % (Calcd: C, 65.93; N, 7.69; H, 4.43. Found: C, 63.25; N, 7.36; H, 4.59). All experiments were performed using analytical grade reagents. Hydrochloric acid solutions [(1 and 6.25) M] were obtained from Sigma-Aldrich. Triethylamine (TEA) and 1-octanol were obtained from Fluka. Deionized water was obtained from a Barnstead NANOpure water system (Barnstead, Dubuque, IA).

HPLC Instrumentation. The HPLC used for drug content analysis consisted of a Waters HPLC system (Milford, MA) equipped with a 717 plus autosampler, a 474 scanning fluorescence detector, an interface module, and a single 515 pump. Chromatographic analysis of 10-HC-lactone and 10-HC-carboxylate species was conducted on an Agilent Zorbax C18 analytical column (4.6 mm × 250 mm, pore size 5 μm), using a mobile phase consisting of a 70:30 (v/v) mixture of aqueous phase to acetonitrile. The aqueous phase consisted of TEA at volume fractions of 1.5 %, with the pH adjusted to 5.5 using acetic acid.[12] Fluorescence detection was carried out with excitation and emission wavelengths set at (382 and 550) nm, respectively, with the flow rate set at 1 mL·min^{-1}. The chromatographic run-time was 10 min with retention times of (3.1 and 6.0) min for 10-HC-carboxylate and 10-HC-lactone, respectively. Calibration curves of 10-HC-lactone and 10-HC-carboxylate were constructed with standard solutions in 0.001 M HCl and 0.001 M NaOH, respectively.

Equilibrium Hydrolysis. Various buffer solutions of pH in the range 3 to 10 were prepared by mixing different proportions of 0.2 M phosphate (Na_2HPO_4) and 0.1 M citric acid solutions. To those, appropriate volumes from stock solutions of the drug in DMSO (2.8 mM) were added, at a constant final 10-HC concentration of 0.82 μM. Samples in triplicate were kept in a thermostatted orbital shaker-type water bath for 120 h (equilibrium was reached within 72 h), after which time 10-HC-lactone and 10-HC-carboxylate were simultaneously quantified using an HPLC assay. Equilibrium hydrolysis data were fitted by eq 1 using the Microsoft Excel solver function, through minimization of the sum of the squared residuals with one adjustable parameter at 5 % tolerance.

$$f = \frac{100}{1 + 10^{(A)*(\mathrm{pH}-B)}} \tag{1}$$

where f is the fraction 10-HC-lactone·100 or the fraction 10-HC-carboxylate·100, at equilibrium; A is either 1 or −1; and B is the adjustable parameter, which refers to the pH at which equilibrium concentrations of 10-HC-lactone and 10-HC-carboxylate are equal.

pK$_a$ Studies. A Cary-eclipse UV-spectrophotometer (Varian Inc., Walnut Creek, CA) equipped with a thermostatted cuvette holder was used to record the spectral scans of 10-HC in different pH solutions. Various pH solutions, all containing 1.9 μM of 10-HC-lactone that was transferred from a 0.2 mM stock solution in DMSO, were made by adding appropriate volumes of 1 M HCl in HPLC grade water. The normalized absorbance values of the spectral scans at λ_{max} of the ionized and the unionized forms were used to calculate the pK_a by eq 1, as described in the previous section. In this case, f and B represent normalized absorption intensity and pK_a, respectively.

Partition Coefficient. The partition coefficient of 10-HC was determined by the shake-flask method.[13] Briefly, 1.1·10^{-8} moles of 10-HC from 0.2 mM stock solution in DMSO were added to equal volumes of the aqueous phase and 1-octanol, in 15 mL capacity, 17 mm × 100 mm, polypropylene conical tubes. Aqueous phases were adjusted to different pH as previously described. Following 24 h of vigorous shaking using an orbital shaker at room temperature, the samples were allowed to equilibrate for another 24 h, after which time the aqueous phase was analyzed for drug concentration. The concentration of 10-HC in octanol was determined from the difference of the total amount of drug added and the amount present in the aqueous phase.

Apparent partition coefficients (P_{app}) were calculated from the ratio of the measured concentrations of 10-HC in the octanol (C_o) and aqueous phase (C_w), according to the following equation

$$P_{app} = \frac{[10 - \mathrm{HC} - \mathrm{lactone}]_o}{[10 - \mathrm{HC} - \mathrm{lactone}]_w + [10 - \mathrm{HCH} - \mathrm{lactone}]_w^+} \tag{2}$$

To obtain initial estimates of the intrinsic partition coefficient of 10-HC, defined as $P = [\text{10-HC-lactone}]_o/[\text{10-HC-lactone}]_w$, eq 2 was appropriately converted to its inverse form.

$$\frac{1}{P_{app}} = \frac{1}{P} + \frac{1}{P \cdot K_a} \cdot [H^+] \tag{3}$$

Final values of the intrinsic partition coefficient of the unionized and ionized form, P and P', respectively, with $P' = [\text{10-HCH-lactone}]_o^+/[\text{10-HCH-lactone}]_w^+$, were obtained from nonlinear fitting of the experimental data by eq 4.[14]

$$P_{app} \cdot \left(1 + \frac{K_a}{[H^+]}\right) = P' + P \cdot \left(\frac{K_a}{[H^+]}\right) \tag{4}$$

Solubility Studies. Excess 10-HC powder was suspended in 25 mL of dissolution media in Kontes jacketed beakers connected to a water circulator (VWR brand, model 1162, Polyscience, IL) for temperature control. The pH of the dissolution media was adjusted at 0.5 to 2 using an appropriate amount of 1 M HCl. Ionic strength, I, was adjusted at 0.31 M with NaCl to match that of the most acidic solution (pH 0.5). Most importantly, the measured pH of these solutions (using Ag/AgCl pH electrode and ATC probe) did not change with temperature, indicating that the activity of HCl was constant within the temperature range used in this experiment. Aqueous solutions having pH < 0.5 were prepared using 6.25 M HCl, without adjusting the ionic strength. The suspensions were stirred for a period of (24 to 36) h, and subsequently, the samples were filtered (Whatman filters, 25 mm diameter, 0.22 mm pore size, VWR scientific) and analyzed by HPLC. To estimate the intrinsic solubility and pK_a of the drug, solubility studies were conducted in pH solutions around the pK_a, namely, 0.5, 0.75, 1, 1.5, and 2. Dissolution experiments were also conducted at various temperatures to gain more insight into the effect of temperature on the solubility of 10-HC-lactone.

The 10-HC concentrations measured within the pH range of 0.5 to 2 were plotted against the calculated hydronium ion concentration, [H$^+$], and data were fitted by eq 5 using linear regression analysis. The intrinsic solubility of the 10-HC free base and the dissociation constant K_a were determined from the intercept and slope of the equation, respectively.

$$C_T = [10 - \mathrm{HC} - \mathrm{lactone}] + \frac{[10 - \mathrm{HC} - \mathrm{lactone}]}{K_a} \cdot [H^+] \tag{5}$$

Total solubility of 10-HC is defined as $C_T = [\text{10-HC-lactone}] + [\text{10-HCH-lactone}]^+$, where $[\text{10-HCH-lactone}]^+$ denotes the protonated form of 10-HC and [H$^+$] is the molar concentration of HCl.

Scheme 3. Static Disk Intrinsic Dissolution Apparatus

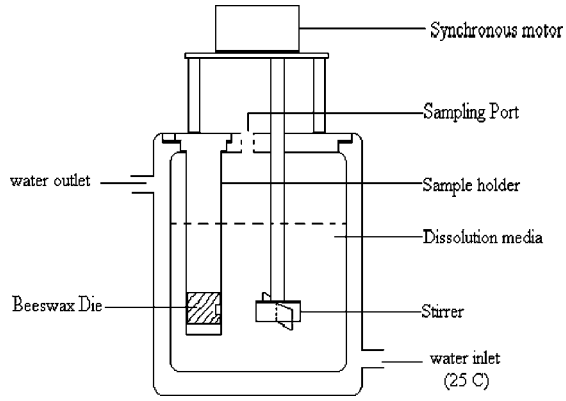

Intrinsic Dissolution Studies. Compacts (surface area = 0.385 cm^2) of benzoic acid and 10-HC were prepared using a hydraulic press (Carver press-2822; Wabash, IN) with a compression force of 34 MPa applied for a period of 10 s to ensure sufficient compaction. The surface area was calculated by measuring the diameter of the compacts using a Vernier caliper. The compacts were then removed from the die and placed into beeswax molds so that only one surface of the tablet is exposed to the media allowing for a constant surface area throughout the dissolution process (Scheme 3). The fixed position of the tablet holder and the stirrer blade ensured constant hydrodynamic conditions during dissolution.[15] The dissolution experiment was started by immersing the tablet holder into the pre-equilibrated media (300 mL) contained in a water-jacketed beaker with the temperature of the media maintained at 25 °C. The dissolution media for benzoic acid was 0.01 M HCl pH 2, with the ionic strength adjusted at 0.5 M using KCl, while that for 10-HC-lactone and 10-HC-lactone hydrochloride salt was 10^{-4} M HCl pH 4, of ionic strength 0.31 M adjusted with NaCl. At predetermined time points, 10 mL aliquots were withdrawn and analyzed for benzoic acid and for 10-HC-lactone using UV-spectrophotometry and HPLC, respectively. The volume in the test vessel was kept constant at all times by replenishing with equal volumes of dissolution media. Dissolution rate constants were determined using the static disk method at (60, 120, 200, 400, and 600) rpm corresponding to the Reynolds numbers ($R_e = (r^2\omega/\nu)$) between 79 and 788 implying a laminar flow at the disk surface.[16] The effects of disk preparation variables (e.g., compression force), volume of dissolution media, and the die position relative to the stirrer, etc., on the disk dissolution were not evaluated since disk intrinsic dissolution rate (DIDR) measurements are considered to be robust with insignificant effect of such experimental variables.[17] The flux of the mass transfer, J, is related to the square root of the rotational speed, ω, expressed in units of rad·s^{-1}, according to the following Levich equation.[16]

$$J = 0.62 \cdot D^{2/3} \cdot C_s \cdot \nu^{-1/6} \cdot \omega^{1/2} \quad (6)$$

where D is the diffusivity of the unionized drug in $cm^2 \cdot s^{-1}$; C_s is the saturation solubility in the dissolution media; and ν is the kinematic viscosity of the media equal to $9.77 \cdot 10^{-7}$ $m^2 \cdot s^{-1}$.

X-ray Powder Diffraction (XRPD). Crystals of 10-HC-lactone hydrochloride salt ($C_{20}H_{16}N_2O_5$ HCl) were obtained by equilibrating excess 10-HC powder in a solution of 2.5 M HCl at room temperature for 24 h. The solid phase was then filtered out and washed with 95 % ethanol, followed by air drying until constant weight (elemental analysis: Calcd: C, 59.93; N, 6.99; H, 4.28; Cl, 8.85. Found: C, 56.77; N, 6.50; H, 4.37; Cl, 9.50; Robertson Microlit Laboratories, Madison, NJ).

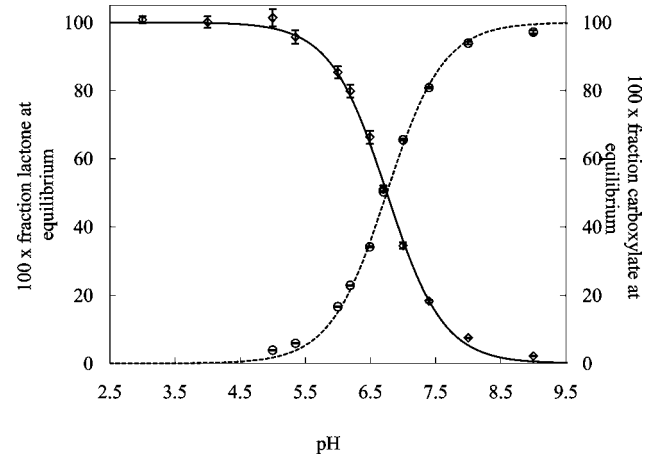

Figure 1. pH profile of the equilibrium concentrations of 10-HC-lactone (◇, primary y-axis) and of 10-HC-carboxylate (○, secondary y-axis), at ambient temperature. Error bars are the standard uncertainties of the average of three experiments. Solid and dashed lines represent best fits of 10-HC-lactone and 10-HC-carboxylate fractions by eq 1, respectively.

Crystals of 10-HC hydrate were obtained after suspending 10-HC powder in pH 4 dissolution media at ambient temperatures. The solid phase was filtered out of solution after 24 h and dried to constant weight. The melting points of 10-HC, 10-HC hydrate, and 10-HC-lactone hydrochloride salt were determined using a Melt-Temp apparatus.

XRPD patterns of the crystals, 10-HC anhydrate and 10-HC hydrate, were registered with a Philips X'Pert system at room temperature. X-rays of 1.54 Å were emanated from a Cu-target, and samples were subjected to a continuous 2θ scan range of 5° to 45° using a scan rate of 1° $\theta \cdot min^{-1}$. Equipment performance was validated using a NIST traceable Mica standard for peak position.

Thermal Analysis. Calorimetric studies were conducted using a differential scanning calorimeter (DSC-Q100, TA Instruments Inc., New Castle, DE) equipped with RCS cooling accessory. The instrument was calibrated using Indium for temperature and enthalpic response. Samples [(5 to 10) mg ± 0.01 mg] were accurately weighed and sealed in aluminum hermetic pans. Experiments were conducted at a heating rate of 10 °C per minute under nitrogen purge from ambient to 300 °C. Onset and peak temperatures and the enthalpy of fusion were determined using Universal analysis software. Thermogravimetric analysis (TGA; Q500, TA Instruments Inc.) of the samples was performed in the same temperature range and at the same heating rate as the DSC studies.

Results and Discussion

Equilibrium Hydrolysis. Equilibrium hydrolysis results are depicted in Figure 1. On the basis of the nonlinear curve fitting of the 10-HC-lactone and 10-HC-carboxylate equilibrium concentrations by eq 1, the following observations can be made: First, the 10-HC is stable as lactone below pH 5. A reversible and exponential decrease in the equilibrium lactone concentration is evident from pH 5 to 7, with only 18 % of 10-HC-lactone remaining at the physiologically relevant pH of 7.4. Second, at and above pH 9, 10-HC is exclusively present in its inactive carboxylate form.

pK_a Studies. Similar to the quinoline, the absorption spectra of 10-HC in the range of (240 to 450) nm consist of four bands with a λ_{max} at 380 nm, and naturally, changes in the ionization state of the quinoline moiety should be reflected in the absorption spectra[18] (Figure 2A). Strel'tsov et al.[19] reported the

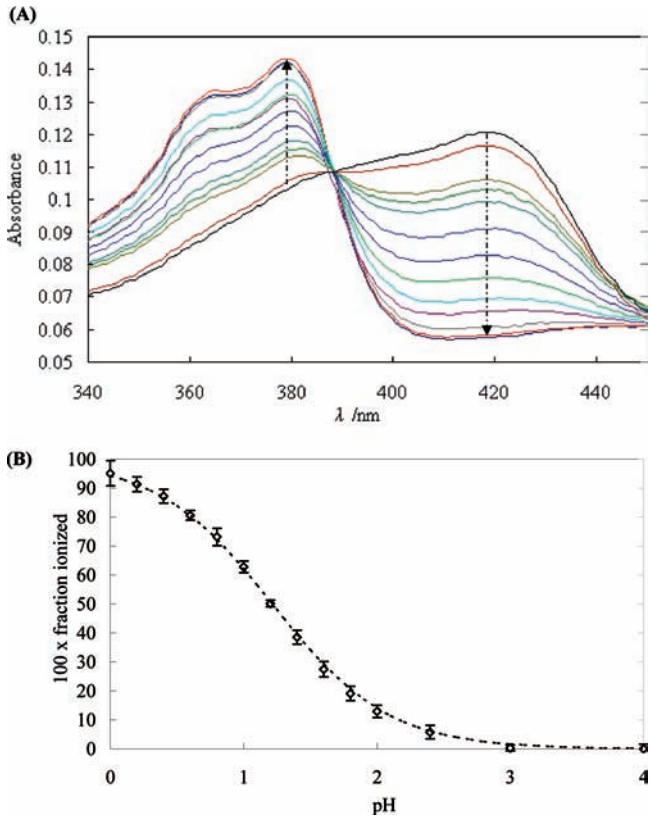

Figure 2. (A) pH-dependent changes of the UV-absorption scans of 10-HC (1.9 μM) at 37 °C. The direction of the arrows indicates increasing pH from 0.1 to 4. (B) Normalized absorbance at 416 nm plotted against the calculated pH values. The results are the average of three independent experiments with the error bars representing standard uncertainty.

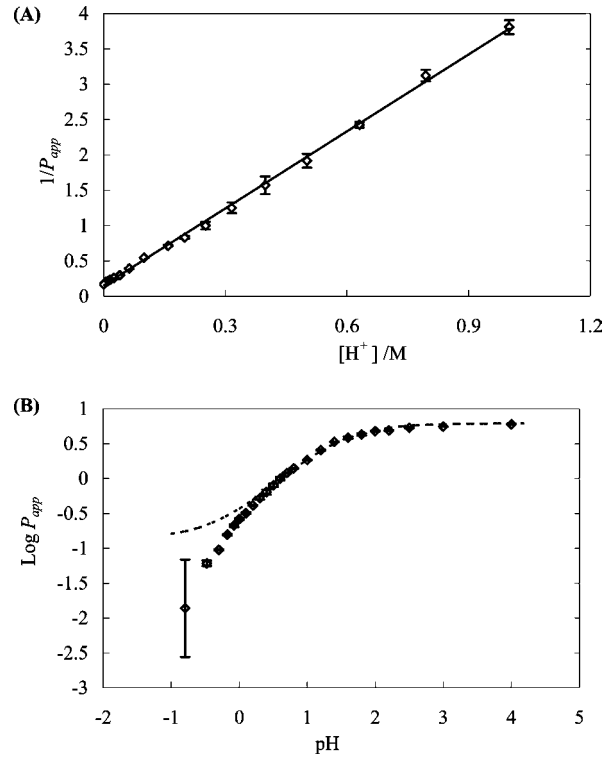

Figure 3. (A) Inverse apparent partition coefficients of 10-HC measured at ambient temperature are plotted as a function of hydrogen ion concentration ([H^+]). Data were fitted by eq 3 (solid line). (B) Measured apparent partition coefficients (empty diamonds) are compared to the simulated fit (broken line) using the logarithmic version of eq 4 ($n = 3$).

presence of two ionizable groups within the ring structure of topotecan, that is, the quinoline nitrogen and the N4 atom, with pK_a of 0.8 and 3.6, respectively. Examining the UV-spectra of 10-HC at different pH within the range of 0.2 to 4, only one isosbestic point is evident indicating the presence of just two species, i.e., protonated and unprotonated quinoline nitrogen of the 10-HC-lactone. By fitting the representative absorbance values as a function of pH to the modified Henderson−Hasselbalch equation (eq 1), the average pK_a of the quinoline nitrogen was found to be 1.23 at 37 °C (Figure 2B). As expected, the extended conjugation of the ring system renders 10-HC a weaker base since the dissociation constant of the unsubstituted quinoline is around 4.85.[20]

Partition Coefficient. To obtain an estimate of the intrinsic partition coefficient of the unprotonated species, measured apparent partition coefficients were fitted by eq 3 using linear regression analysis of the data ($r^2 = 0.997$), as shown in Figure 3A. From the slope and intercept, the pK_a and P were determined to be 1.37 ± 0.03 and 6.49 ± 0.4, respectively. The P value obtained from eq 3 was then applied to eq 4, which accounts for possible partitioning of the ionized drug into the organic phase. The intrinsic partition coefficient of the ionized form [10-HCH-lactone]$^+$, P', was calculated to be equal to 0.04. Careful inspection of Figure 3B indicates that results fitted in accord to the logarithmic version of eq 4 deviated from measured P_{app} values at pH < 0.5. Although similar behavior was noted with the parent camptothecin (CPT) molecule,[14] the much higher P value of CPT (52 versus 6.2) suggests that the hydroxyl group substitution greatly increases the polar surface area (PSA) of the molecule with a negative impact on cell membrane permeability.

Solubility Studies. Apparent equilibrium solubility C_T, measured at various temperatures, was plotted as a function of pH, and the results were fitted in accordance with eq 5 (Figure 4A), thus allowing the intrinsic solubility of 10-HC-lactone and pK_a to be calculated from the intercepts and slopes of the various isotherms, respectively. Due to the endothermic nature of the dissolution process, the intrinsic solubility of the unionized lactone increased with temperature to about 3 times its magnitude from (25 to 45) °C (Figure 4B). Moreover, the intrinsic solubility of 10-HC at 25 °C was found to be 1.81 μM as compared to a bigger value of 3.44 μM for CPT. However, the much higher ionic strength of 10-HC solubility experiments does not allow a direct comparison of these values, and thus the results are not contradictory given the increased polarity of the 10-HC. Contrary to that, the apparent pK_a was found to decrease with increasing temperatures (Figure 4C). This inverse relationship of pK_a with temperature indicates that the ionization or the protonation of 10-HC-lactone is suppressed; i.e., the basicity of the drug decreases as temperature increases. As mentioned earlier, the measured pH values were unaffected by temperature changes, signifying that the activity of HCl remained unaltered within the temperature range used in this study. Evidently, the temperature dependence of pK_a is related only to the temperature effects on the protonation−deprotonation reactions of 10-HC. It is worth noting that the pK_a calculated from the equilibrium solubility data at 25 °C is in close agreement with that calculated from the direct titration and octanol−water 10-HC partitioning.

The intrinsic solubilities of the unionized species shown in Table 1 were plotted against the inverse absolute temperature (Figure 4B). The data were fitted by the integrated form of the Gibbs−Helmholtz equation shown below. Evaluation of the slope of the linear fit based on eq 7 yielded an average standard

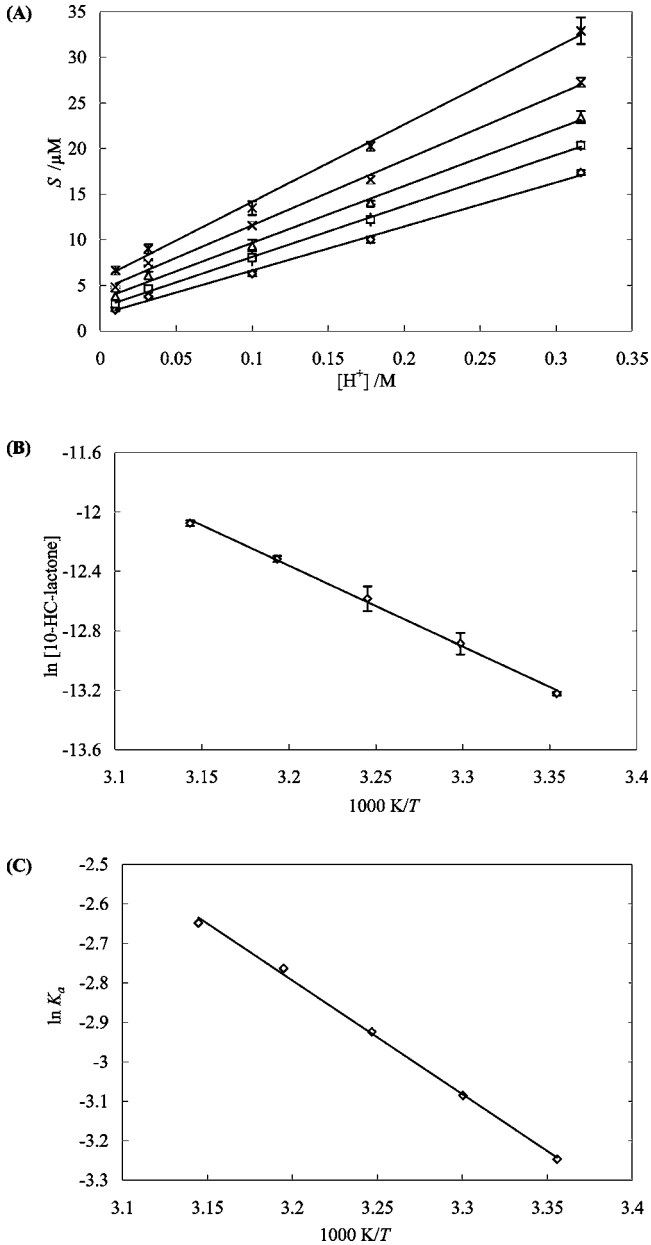

Figure 4. (A) Isotherms of saturated concentration of 10-HC versus hydrogen ion concentration, $[H^+]$, at ◇, 25 °C; □, 30 °C; Δ, 35 °C; ×, 40 °C; ∗, 45 °C ($n = 3$). (B) Intrinsic solubility of the unionized form [10-HC-lactone] plotted against the inverse absolute temperature. (C) van't Hoff plot depicting the linear dependence of ln K_a with inverse temperature. Symbols are the average of three experiments, whereas error bars represent standard uncertainties.

enthalpy of solution of the unprotonated species 10-HC-lactone equal to 45.16 kJ·mol^{-1}.

$$\ln[10 - \mathrm{HC} - \mathrm{lactone}]_{sat} = -\frac{\Delta_{sol}H'^{o}_{un}}{R} \cdot \frac{1}{T} + C(T) \quad (7)$$

where $[10\text{-HC-lactone}]_{sat}$ and $\Delta_{sol}H'^{o}_{un}$ are the saturated concentration of the unionized lactone species and the apparent standard enthalpy of solution of 10-HC-lactone, respectively. The constant $C(T)$ is a function of the variable, namely, the temperature, that was held constant to obtain the total differential of the Gibbs free energy, the Gibbs−Helmholtz equation $\partial/\partial T[\Delta_{sol}\mu^o/T]_{P,I} = -\Delta_{sol}\bar{H}^o/T^2$, where $\Delta_{sol}\mu^o$ is the standard chemical potential of solution of 10-HC-lactone evaluated at constant pressure and ionic strength, and $\Delta_{sol}\bar{H}^o$ is the standard partial molar enthalpy of solution.

Table 1. (Top) Intrinsic Solubility of Unionized Species and Ionization Constants as a Function of Temperature and (Bottom) Enthalpy of Solution $\Delta_{sol}H'^o$ of (Ionized + Unionized) Species as a Function of pH[a]

T/K	pK_a	intrinsic solubility/μM
298.15	1.42 ± 0.01	1.81 ± 0.02
303.15	1.34 ± 0.05	2.54 ± 0.2
308.15	1.26 ± 0.05	3.43 ± 0.3
313.15	1.20 ± 0.01	4.47 ± 0.09
318.15	1.17 ± 0.03	5.69 ± 0.1

pH	$\Delta_{sol}H'^o$/kJ·mol^{-1}
0.50	24.8 ± 1.3
0.75	27.1 ± 0.5
1.0	29.8 ± 2.0
1.50	35.2 ± 1.8
2.00	40.8 ± 3.8

[a] Values reported are the averages of three independent experiments ± standard uncertainties.

Scheme 4. Ionization Reaction of Quinoline Nitrogen of 10-HC

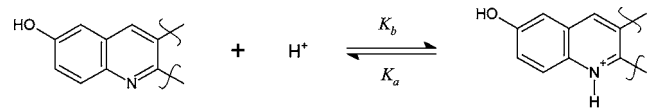

10 – HC – lactone (10 – HCH – lactone)$^+$

Complete ionization of the quinoline nitrogen of the 10-HC-lactone is expected to take place at least 2 pH units below the apparent pK_a (Scheme 4).

Since this is an equilibrium reaction, a plot of ln K_a as a function of inverse temperature should result in a straight line with the apparent standard heat of deprotonation, $\Delta_{dep}H'^o$, being the slope of the fitted data in accord to eq 8

$$\frac{\partial}{\partial T}[\ln K_a] = -\frac{\Delta_{dep}H'^{o}}{R \cdot T^2} = \frac{\Delta_{ion}H'^{o}}{R \cdot T^2} \quad (8)$$

The standard enthalpy of deprotonation of 10-HC-lactone was calculated from three independent experiments to be (23.6 ± 2.2) kJ·mol^{-1} (Figure 4C). The negative heat involved in the protonation or ionization of quinoline nitrogen is reflective of the increased resistance of the molecule to gain a proton and provided a thermodynamic explanation of the decreased basicity of 10-HC-lactone with increasing temperature.

Similarly, the temperature dependence of equilibrium solubility of 10-HC at different pH is depicted in Figure 5A. The slopes of the various iso-pH lines were evaluated to obtain the apparent standard enthalpy of solution $\Delta_{sol}H'^o$ containing both unionized and protonated 10-HC-lactone molecules (Table 1). In general, evaluation of the enthalpy of solution from the slope of the linear fits is safe and reasonably accurate because its actual value is independent of the choice of the reference function. A plot of the $\Delta_{sol}H'^o$ against the fraction ionized f_{ion} and a least-squares fitting of the data in accord to eq 9, allowed us to calculate an average value of the apparent standard heat of solution of the ionized lactone species, $\Delta_{sol}H'^{o}_{ion}$, equal to 22.7 kJ·mol^{-1} at 25 °C (Figure 5B). Thus, although the solubility of both species is an endothermic process, the dissolution of protonated species is evidently less dependent on temperature.

$$\Delta_{sol}H'^o = (\Delta_{sol}H'^{o}_{ion} - \Delta_{sol}H'^{o}_{un}) \cdot f_{ion} + \Delta_{sol}H'^{o}_{un} \quad (9)$$

Solution formation and ionization of 10-HC-lactone in acidic media is summarized in Scheme 5. It is important to recognize

that standard enthalpies of solution are the difference measurements of the standard partial molar enthalpies of formation of the substance solution, $\Delta H^{o}_{f,S(sol,\infty)}$. The first reaction (R1) describes the dissolution of solid 10-HC-lactone in water. Although experiments were carried out in aqueous solutions containing dilute concentrations of HCl for adjustment of pH, R1 is justified because the intrinsic solubility of unionized species was evaluated from the intercept of the linear fit of the data shown in Figure 4A, that is, at infinite dilution where essentially the concentration of HCl is zero. Reactions 2 and 3 described the formation and dissolution of HCl, respectively. The sum of the two reaction heats is equal to the standard enthalpy of formation of HCl in the solution state. Since ionic compounds ionize fully in infinitely dilute aqueous solutions, HCl should exist in the form of the corresponding ions in solution. Furthermore, the enthalpy of formation of the HCl solution should be equal to the enthalpies of formation of the corresponding ions in solution (R4). Finally, R5 describes the ionization of dilute 10-HC-lactone solution in acidic media. As shown in Scheme 5, although protonation of the weak base is exothermic, the dissolution process for the ionized lactone species is endothermic because the absolute value of the negative heat of ionization $\Delta_{ion}H'^{o}$ (-23.9 kJ·mol^{-1}) is so much smaller than the $\Delta_{sol}H'^{o}_{un}$ (45.4 kJ·mol^{-1}). As a result, equilibrium solubility of both ionized and unionized species increases with increasing temperatures.

To better evaluate the effect of pH on apparent solubility of 10-HC, saturated concentrations of 10-HC were measured in extremely acidic media (pH < 0.5) at 298.15 K and plotted as a function of pH using eq 5 in the form $C_T = [10{-}HC{-}lactone]\cdot\{1 + 10^{(pK_a - pH)}\}$. In principle, equilibrium solubility should increase exponentially and reach a maximum value at pH = pH_{max} where the solubility product $K_{sp} = [10{-}HCH{-}lactone]^{+}$ is reached. In Figure 6, at pH = pH_{max}, a plateau line is arbitrarily drawn since pH values smaller than pH_{max} fall outside the valid domain of eq 5. As it is also portrayed in the same figure, the solubility of 10-HC is accurately described by this equation at slightly acidic pH but deviates significantly from the anticipated profile at pH < 0.5. More specifically, the equilibrium solubility at pH corresponding to [H$^+$] = 4 M was found to be 3 mM as compared to the 40 times lower maximum solubility of 125 μM predicted by eq 5. It needs to be mentioned that the occurrence of K_{sp} below the pH_{max} was verified by first preparing

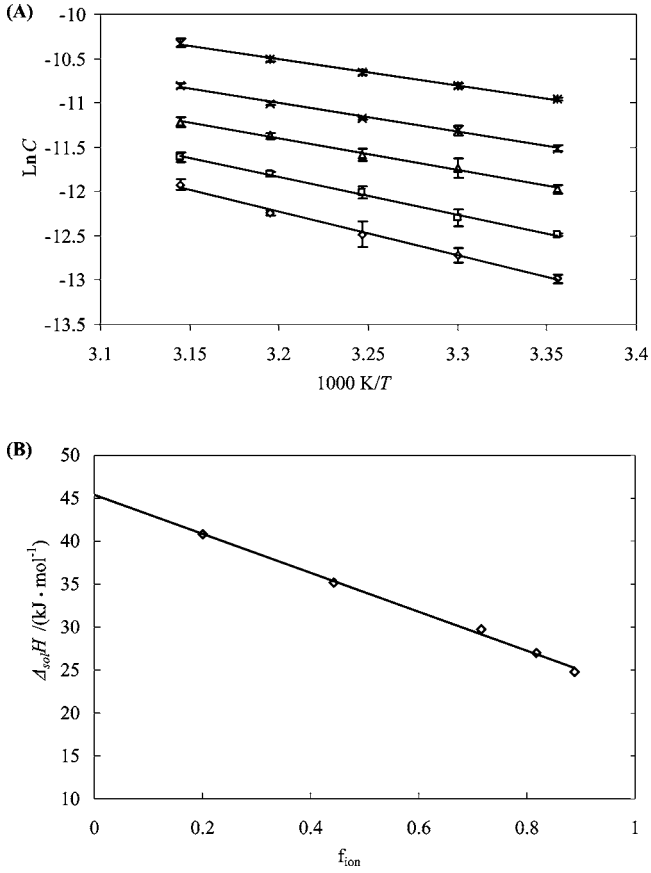

Figure 5. (A) Iso-pH plots of 10-HC saturated concentration against inverse temperature in pH ◇, 2; □, 1.5; Δ, 1; ×, 0.75; ∗, 0.5. (B) Plot of enthalpy of solution as a function of fraction ionized that was calculated from the pK_a value of 10-HC using the Henderson−Hasselbalch equation.

Scheme 5. Summary of Chemical Reactions and Heats Involved in Solution Formation and Ionization of 10-HC-Lactone[a]

$$10-HC-\text{lactone (s)} + \infty\ H_2O \rightarrow 10-HC-\text{lactone (sol,}\infty) \qquad \text{R1}$$

$$\Delta_r H^o = \Delta_{sol} H'^o_{un} = 45.16\ \text{kJ}\cdot\text{mol}^{-1}$$

$$0.5\,H_2\ (g) + 0.5\,Cl_2 \rightarrow HCl\ (g) \qquad \text{R2}$$

$$\Delta H^o_{f\,HCl(g)} = -92.31\ \text{kJ}\cdot\text{mol}^{-1}$$

$$HCl\ (g) + \infty\ H_2O \rightarrow HCl\ (sol,\infty) \qquad \text{R3}$$

$$\Delta_{sol} H^o_{HCl} = -74.85\ \text{kJ}\cdot\text{mol}^{-1}$$

$$\text{But} \quad \Delta_{sol} H^o_{HCl} = \Delta H^o_{f\,HCl(sol,\infty)} - \Delta H^o_{f\,HCl(g)}$$

$$\Rightarrow \quad \Delta H^o_{f\,HCl(sol,\infty)} = \Delta_{sol} H^o_{HCl} + \Delta H^o_{f\,HCl(g)} = -167.16\ \text{kJ}\cdot\text{mol}^{-1}$$

$$HCl\ (sol,\infty) \rightarrow H^+\ (sol,\infty) + Cl^-(sol,\infty) \qquad \text{R4}$$

$$\textit{and} \quad \Delta H^o_{f\,HCl\,(sol,\infty)} = \Delta H^o_{f\,Cl^-(sol,\infty)} + \Delta H^o_{f\,H^+(sol,\infty)}$$

$$\text{Defining, } \Delta H^o_{f\,H^+(sol,\infty)} = 0 \text{ as the reference point,}$$

$$\Delta H^o_{f\,Cl^-(sol,\infty)} = \Delta H^o_{f\,HCl\,(sol,\infty)} = -167.16\ \text{kJ}\cdot\text{mol}^{-1}$$

$$10-HC-\text{lactone (sol,}\infty) + H^+\ (sol,\infty) + Cl^-(sol,\infty) \rightarrow 10-HC-\text{lactone}-H^+\ (sol,\infty) + Cl^-(sol,\infty) \qquad \text{R5}$$

$$\Delta_r H'^o = \Delta_{ion} H'^o = \Delta H'^o_{f\,10-HC-\text{lactone}-H^+(sol,\infty)} - \Delta H'^o_{f\,10-HC-\text{lactone (sol,}\infty)}$$

$$\textit{or} \quad \Delta_{ion} H'^o = \Delta_{sol} H'^o_{ion} - \Delta_{sol} H'^o_{un} \quad \Rightarrow \quad \Delta_{sol} H'^o_{ion} = 21.5\ \text{kJ}\cdot\text{mol}^{-1}$$

[a] Standard enthalpies of formation and ionization for HCl at 298.15 K were extracted from the Handbook of Chemistry and Physics, 78th ed., CRC Press, Boca Raton, FL, 1997−98. Superb analysis of computing enthalpy changes of reactions in solutions is contained in Raff's Physical Chemistry.[21]

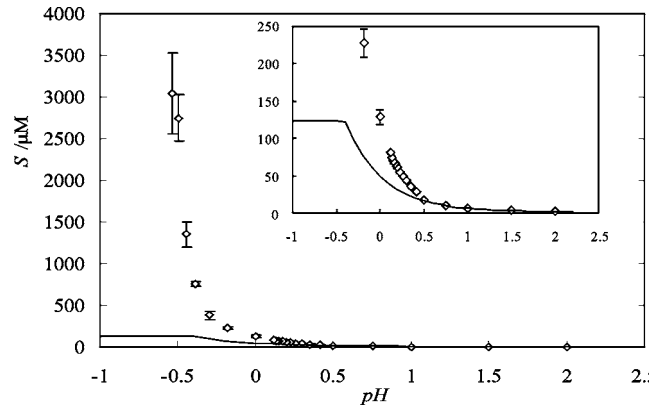

Figure 6. Plot of molar solubility, *S*, of 10-HC as a function of pH at 298.15 K. Deviation from predicted values in accord to eq 5 at pH < 0.5 is clearly shown in the inset. The average and the standard uncertainties shown are from three independent experiments.

Table 2. Intrinsic Solubility and Diffusivity Data for Benzoic Acid and 10-Hydroxy-camptothecin Calculated from Intrinsic Dissolution Studies[a]

		intrinsic solubility	slope	calculated diffusivity	
compound	pK_a	M	$ng \cdot cm^{-2} \cdot s^{-1/2}$	$cm^2 \cdot s^{-1}$	r^2
benzoic acid	4.03	$2.14 \cdot 10^{-2}$	$1.63 \cdot 10^{-3}$	$1.01 \cdot 10^{-5}$	0.999
10-HC	1.42	$1.81 \cdot 10^{-6}$ [b]	$0.49 \cdot 10^{-6}$	$1.30 \cdot 10^{-5}$ [b]	0.993

[a] Intrinsic solubilities were determined in respective dissolution media. The diffusivities were calculated from the slopes of Levich plots according to eq 9. [b] Intrinsic solubility and diffusivity are for the monohydrate form of 10-HC.

supersaturated solutions of 10-HC in 2.5 M HCl at 45 °C, followed by cooling the solution to room temperature which led to the precipitation of 10-HC−HCl salt (elemental analysis $C_{20}H_{16}N_2O_5 \cdot HCl \cdot H_2O$, Calcd: C, 57.35; N, 6.69; H, 4.57; Cl, 8.47. Found: C, 57.13; N, 6.58; H, 4.45; Cl, 9.02). Thus, the solid phase in equilibrium with 10-HC saturated solutions is a 10-HC−lactone−monohydrate HCl salt. The saturated solutions prepared at pH lower than 0.5 were stable at room temperature for at least one week without any drug precipitation, and consequently, the increased solubility is not due to the formation of metastable or supersaturated solutions close to the pH_{max}.[22] The extraordinarily high solubility observed in extremely acidic media is attributed to the increased solvency of the concentrated acid solutions toward the protonated 10-HC-lactone salt, as previously noted for camptothecin.[14] Specifically, the solubility of CPT in 1 M HCl was determined to be (45.4 ± 0.5) $mg \cdot L^{-1}$ as compared to the very similar value of 47.05 $mg \cdot L^{-1}$ for 10-HC. This exponential increase in the drug solubility in concentrated acid (> 1 M) could be used to formulate colloidal systems with improved 10-HC stability.

Intrinsic Dissolution Studies. The dissolution of benzoic acid is diffusion-controlled, and so, it was used as a standard compound to validate the apparatus. The saturated concentration C_s of benzoic acid at pH 2 and ionic strength 0.5 M was determined to be $2.14 \cdot 10^{-2}$ M, while the diffusivity of benzoic acid was calculated using eq 6 to be $1.01 \cdot 10^{-5}$ $cm^2 \cdot s^{-1}$ (Table 2), in good agreement with the previously reported value.[23]

Unlike benzoic acid, the intrinsic dissolution profile of 10-HC was clearly biphasic having two distinct slopes irrespective of rpm (Figure 7A). The slope of the initial portion of the dissolution curve (from (0 to around 90) min) was on average 1.68 times higher than that of the later part (Figure 7B). To shed light on the biphasic nature of the dissolution profile, the diffraction patterns of 10-HC anhydrous and 10-HC monohydrate (crystal formation as described in the Methods section) were evaluated (Figure 8). The differences in the peak positions in the overlay plot and the respective intensities are apparent, suggesting that the two different dissolution rates might be due to solid state transformation of 10-HC at the surface of the disk. Most importantly, a nondiffusion-controlled dissolution is unlikely in view of the zero flux obtained at zero stirring rates of both phases (intercepts of linear fits of Figure 7B).

In the present context, the two different crystalline states are referred to as Form I and Form II. Equilibrium solubility studies allowed us to calculate the saturated concentration of Form II (S_{II}) equal to 1.81 μM. Assuming the same diffusion coefficient for Form I and Form II, the solubility of Form I (S_I) was calculated by evaluating the corresponding dissolution rate dC/dt using

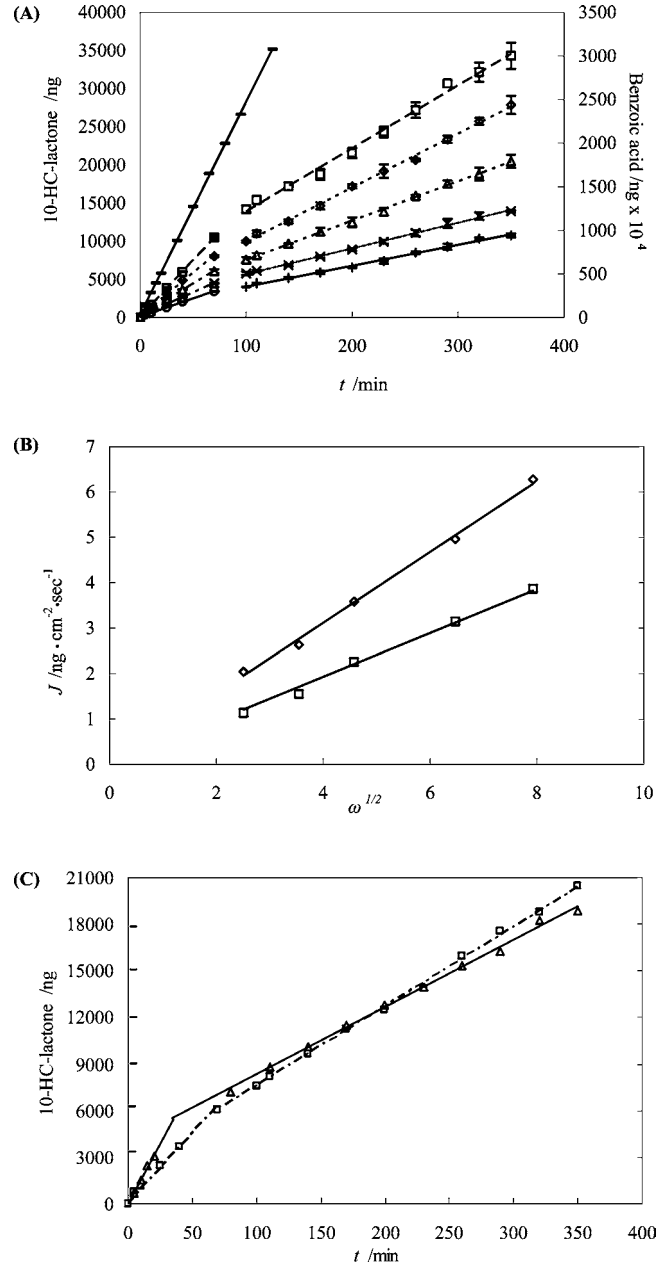

Figure 7. (A) Intrinsic dissolution profiles of 10-HC at different shaft rotational speeds (+, 60; ×, 120; Δ, 200; ◇, 400; and □, 600) at 25 °C. The dissolution rate for latter time points was ∼ 40 % less compared to the initial dissolution rate. For comparison, the intrinsic dissolution profile of benzoic acid at 600 rpm (−) is also shown (secondary *y*-axis). (B) Levich plot of the flux, *J*, of 10-HC calculated from the initial (top; Form I) and later (bottom; Form II) time points as a function of the square root of rotational speed, $\omega^{1/2}$. (C) Intrinsic dissolution profile of 10-HC-HCl salt (−) compared to that of 10-HC anhydrous (-•-•) at a stirrer speed of 200 rpm and 25 °C in 10^{-4} M HCl, $I = 0.31$ M.

$$S_I = \left(\frac{(dC/dt)_I}{(dC/dt)_{II}} \right) \cdot S_{II} \qquad (10)$$

The above-mentioned relation is based on the principle of the dissolution rate constant for both forms being proportional to the diffusion coefficient of 10-HC, boundary layer thickness, and the surface area of dissolving solid.[24] On the basis of the linear relationship between the square root of angular velocity, ω, and the flux, *J* (Figure 7B), it is apparent that the dissolution of both forms of 10-HC is diffusion controlled. Since hydrodynamic conditions and the integrity of the disk (constant surface

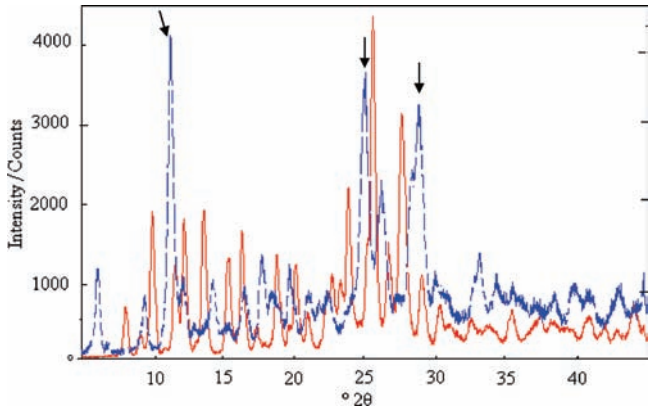

Figure 8. Overlaid XRD patterns of 10-HC anhydrate (—) and 10-HC-monohydrate (top diffractogram, dashed line). Arrows indicate prominent peaks of the 10-HC monohydrate.

area) remain unchanged during the dissolution process, it is safe to assume similar diffusion coefficients for both Form I and Form II. The solubility of Form I thus calculated was 2.95 μM.

With respect to the intrinsic dissolution profile of 10-HC-HCl, the initial dissolution, from (0 to 20) min was 4 times faster than the latter times (Figure 7C). After approximately 2 h, the dissolution profile was similar but not identical to that of Form II. The presence of a distinctly different crystal structure was verified by XRD (diffractogram not shown), DSC, and melting point determination.

Solid State Characterization. Thermal analysis was done for three samples. Sample 1: 10-HC powder as received from the vendor. Sample 2 and Sample 3: the dried solid phases following powder dissolution of 10-HC in pH 4 and in highly acidic ([H^+] > 2.5 M) dissolution media, respectively. The overlaid thermograms are presented in Figure 9.

The thermal events of 10-HC consist of an endotherm centered at 194 °C, followed by an exothermic peak at 240 °C and a consecutive endothermic−exothermic transition, in that order, at around 278 °C. Thermal gravimetric analysis (TGA) of the sample revealed that a relative mass loss of 4.69 % took place from (40 to 65) °C and an additional relative mass loss of 11.9 % within the temperature range of (270 to 305) °C, corresponding to stoichiometric thermal decarboxylation of 10-HC. The relatively low temperature associated with the 4.69 % loss of relative mass suggests possible removal of residual organic solvent from the crystalline sample. The fact that TGA indicated no relative mass loss within the temperature range of (70 to 260) °C suggests that the first endothermic event observed on DSC at 194 °C is the crystalline-to-liquid phase transition of the compound ($\Delta_{fus}H$ = 53.38 kJ·mol^{-1}; also verified by melting point determination). The exothermic transition at 240 °C is too small, and it could be partial recrystallization of the melted material. The sequential endothermic and exothermic peaks at 278 °C are representative of thermal decarboxylation of the drug and further structure rearrangements of the decarboxylated product, respectively. This interpretation was based on the fact that bond rupture is energy demanding, while structural rearrangements of the decarboxylated substance could be exothermic in nature and highly probable given the high temperature of the system.[25]

At this point, a word about the possible effects of organic impurities on the equilibrium solubility of the compound is appropriate. As mentioned in the Materials section, the mass fraction purity of the compound was found by our analysis to be 0.96 which is in great agreement with the analysis of the

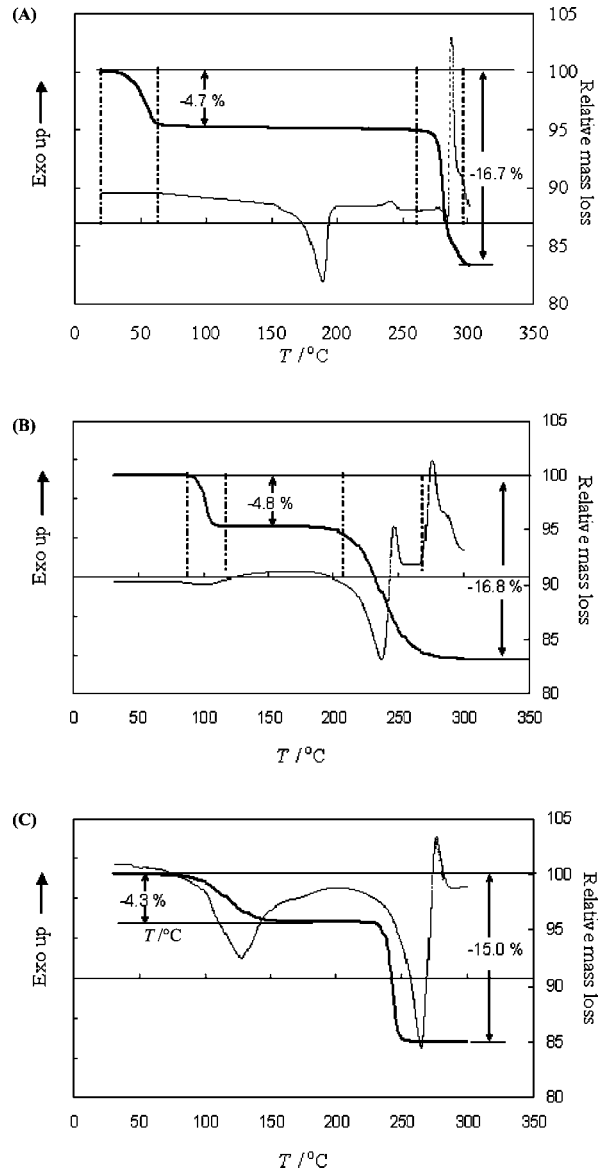

Figure 9. Overlay of TGA (thick line) and DSC (—) thermograms, showing the dehydration, melting, and decarboxylation of (A) 10-HC, (B) 10-HC monohydrate, and (C) 10-HC-HCl salt.

TGA that indicated an impurity equivalent to a fractional mass of 0.0469 as related to the MW of the 10-HC. The fact that the impurity does not show up on the liquid chromatogram and it was removed upon heating the compound at (50 to 70) °C suggests that the impurity could be a volatile organic solvent that is not part of the crystal structure. The solubility studies were carried out with 10 mg of drug in 25 mL of dissolution media corresponding to drug concentration of 1.876·10^{-5} g·mL^{-1} or 18.76 ppm. This quantity is too small to cause changes in the properties of the solvent that could potentially affect the equilibrium solubility of the drug, which is known to be dependent on the crystal structure and solvent properties. Furthermore, the possibility of the impurity affecting the dissolution rate is more common, but the intrinsic dissolution studies indicated that there is no lag time during the initial times of the dissolution studies. These results argue against granule coating by the organic solvent that could potentially slow down the wetting of the powder and the drug release in the aqueous dissolution media.

The TGA and DSC scans of the 10-HC hydrate are shown in Figure 9B. The endotherm shown as a shallow broad peak

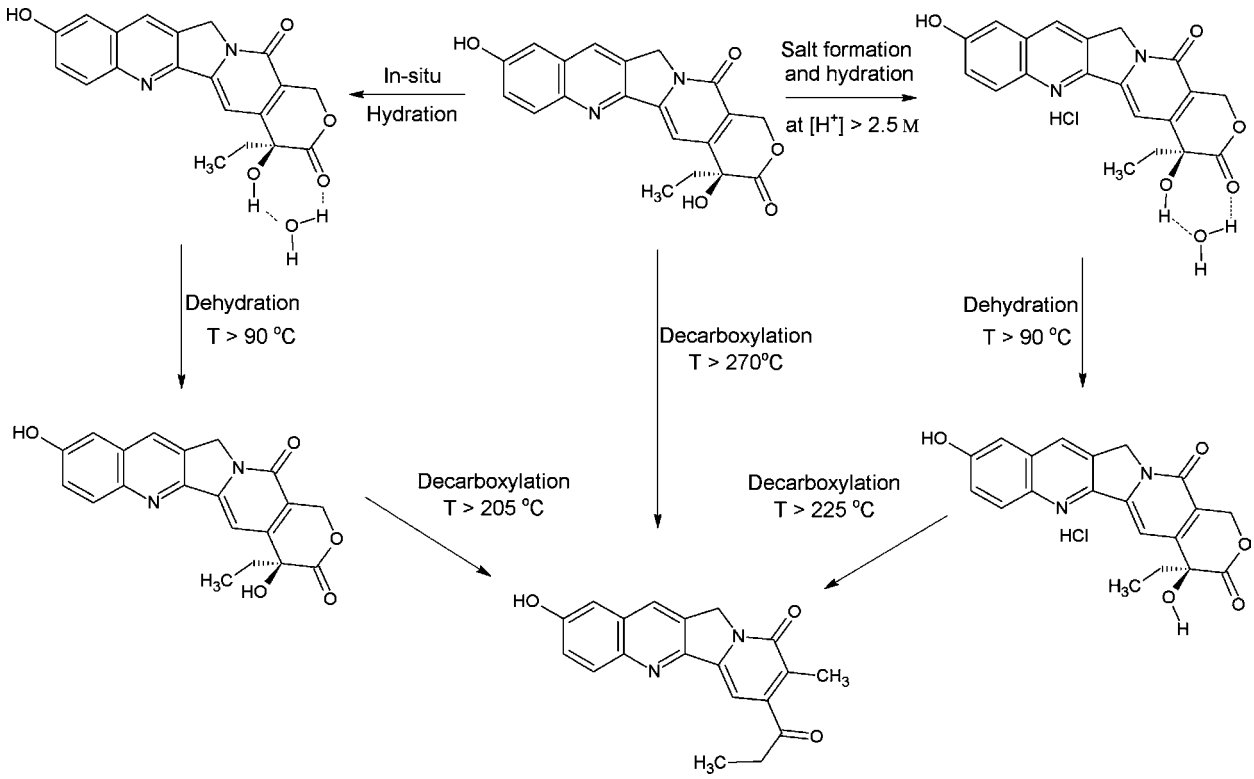

Figure 10. Summary of hydration, salt formation, and thermal events associated with 10-HC.

on DSC is, as indicated by TGA, associated with mass loss at a temperature range of (90 to 110) °C. The 4.75 % relative mass reduction corresponds to the loss of one water molecule per 10-HC molecule, thus supporting the in situ solution-mediated anhydrous-to-monohydrate crystal phase transformation during the intrinsic dissolution studies. Contrary to the fusion of the anhydrous solid, the 10-HC monohydrate crystal exhibited an endothermic transition at around 230 °C. Since TGA indicated a 12.1 % relative mass loss within the (210 to 270) °C temperature range, we conclude that this phase transition represents the combined fusion and decarboxylation of the 10-HC, as described above for the 10-HC anhydrous.

The thermogram of hydrochloride salt also differed significantly from that of 10-HC. Similarly to the 10-HC monohydrate crystal, the two broad endothermic peaks observed at (90 to 150) °C and (220 to 270) °C are both characterized with 4.31 % and 10.7 % relative mass loss corresponding to dehydration and decarboxylation of the sample, respectively. The first rather broad temperature range of relative mass loss could be due to combined bound water and HCl vaporization. An endothermic peak at 267 °C was immediately followed by an exotherm. The melting of 10-HC-monohydrate-HCl salt was not apparent due to simultaneous decarboxylation and melting. Simultaneous melting and decarboxylation of the crystal was confirmed by a melting point apparatus which documented the melting point of the crystal at 260 °C immediately preceded by the discoloration of the sample. Interestingly, the midtemperature of decarboxylation for 10-HC monohydrate and 10-HC HCl salt as detected by TGA is about 40 °C lower than that for 10-HC anhydrous and is similar to the thermal decarboxylation temperature previously reported for 10-HC monohydrate.[25] It is rather surprising that the early fusion event of the anhydrous crystal does not lead to an early decarboxylation event when compared to the monohydrate crystals. On the basis of the above observations, a summary of events and related structures is presented in Figure 10.

Conclusions

The purpose of the present work was to conduct a detailed physicochemical characterization of the 10-HC, in an effort to elucidate formulation strategies that will improve its pharmacological activity. Equilibrium hydrolysis studies in aqueous media indicated that 10-HC is stable in its lactone form at pH $\leq$ 5. The pK_a of the 10-HC-lactone was determined to be 1.23 at physiological temperature and was found to decrease with increasing temperature. Detailed analysis of equilibrium solubility measurements afforded estimates of the enthalpies of dissolution of the ionized and unionized species in aqueous media and provided a thermodynamic explanation for the temperature-dependent basicity of 10-HC. Octanol/water partition studies indicated that in comparison to the parent camptothecin (CPT) the 10-HC is significantly more polar. Nonetheless, the equilibrium solubility of the two molecules was similar, suggesting that this difference in polarity is not translated into increased solubility of the molecule in aqueous media. Finally, intrinsic dissolution, X-ray, and thermal analysis studies revealed the polymorphic nature of 10-HC in aqueous media that could complicate formulating efforts if it is not taken into serious consideration.

Taken together, aqueous solubility, diffusivity, and intrinsic partition coefficient revealed the potential for oral absorption of 10-HC to be dissolution and permeability rate-limited. Use of 10-HC salt to improve the dissolution rate is limited because of its rapid conversion to the free base upon contact with the dissolution media. Moreover, efficient systemic administration of 10-HC will require loading into a delivery vehicle. Unfortunately, apart from being practically insoluble in water, 10-HC is sparingly soluble in most volatile organic solvents. A solution to this problem can come from the increased solvency of 10-HC in extremely acidic media. Formulation of high efficiency delivery systems can be facilitated by using

concentrated acids as a common solvent for both the drug and selected vehicle.

Acknowledgment

We thank Mr. Sohodeb Saha for his valuable contribution in performing XRD and Thermo Gravimetric Analysis.

Literature Cited

(1) Ping, Y. H.; Lee, H. C.; Lee, J. Y.; Wu, P. H.; Ho, L. K.; Chi, C. W.; Lu, M. F.; Wang, J. J. Anticancer effects of low-dose 10-hydroxy-camptothecin in human colon cancer. *Oncol. Rep.* **2006**, *15*, 1273–1279.

(2) Kunadharaju, S.; Savva, M. Kinetic and thermodynamic analysis of 10-hydroxy-camptothecin hydrolysis at physiological pH. *J. Chem. Thermodyn.* **2008**, *40*, 1439–1444.

(3) Wani, M. C.; Ronman, P. E.; Lindley, J. T.; Wall, M. E. Plant antitumor agents. 18. Synthesis and biological activity of camptothecin analogues. *J. Med. Chem.* **1980**, *23*, 554–560.

(4) Gottlieb, J. A.; Guarino, A. M.; Call, J. B.; Oliverio, V. T.; Block, J. B. Preliminary pharmacologic and clinical evaluation of camptothecin sodium (NSC-100880). *Cancer Chemother. Rep.* **1970**, *54*, 461–470.

(5) Jaxel, C.; Kohn, K. W.; Wani, M. C.; Wall, M. E.; Pommier, Y. Structure-activity study of the actions of camptothecin derivatives on mammalian topoisomerase I: evidence for a specific receptor site and a relation to antitumor activity. *Cancer Res.* **1989**, *49*, 1465–1469.

(6) Drewinko, B.; Freireich, E. J.; Gottlieb, J. A. Lethal activity of camptothecin sodium on human lymphoma cells. *Cancer Res.* **1974**, *34*, 747–750.

(7) Burke, T. G.; Mi, Z. The structural basis of camptothecin interactions with human serum albumin: impact on drug stability. *J. Med. Chem.* **1994**, *37*, 40–46.

(8) Zhang, L.; Yang, M.; Wang, Q.; Li, Y.; Guo, R.; Jiang, X.; Yang, C.; Liu, B. 10-Hydroxycamptothecin loaded nanoparticles: preparation and antitumor activity in mice. *J. Controlled Release* **2007**, *119*, 153–162.

(9) Zhang, L.; Hu, Y.; Jiang, X.; Yang, C.; Lu, W.; Yang, Y. H. Camptothecin derivative-loaded poly(caprolactone-co-lactide)-b-PEG-b-poly(caprolactone-co-lactide) nanoparticles and their biodistribution in mice. *J. Controlled Release* **2004**, *96*, 135–148.

(10) Yang, L.; Cui, F.; Cun, D.; Tao, A.; Shi, K.; Lin, W. Preparation, characterization and biodistribution of the lactone form of 10-hydroxycamptothecin (HCPT)-loaded bovine serum albumin (BSA) nanoparticles. *Int. J. Pharm.* **2007**, *340*, 163–172.

(11) Liu, K.; Sun, J.; Wang, Y.; He, Y.; Gao, K.; He, Z. Preparation and characterization of 10-hydroxycamptothecin loaded nanostructured lipid carriers. *Drug Dev. Ind. Pharm.* **2008**, *34*, 465–471.

(12) Warner, D. L.; Burke, T. G. Simple and versatile high-performance liquid chromatographic method for the simultaneous quantitation of the lactone and carboxylate forms of camptothecin anticancer drugs. *J. Chromatogr. B, Biomed. Sci. Appl.* **1997**, *691*, 161–171.

(13) Paschke, A.; Neitzel, P. L.; Walther, W.; Schuurmann, G. Octanol/water partition coefficient of selected herbicides: determination using shake-flask method and reversed-phase high-performance liquid chromatography. *J. Chem. Eng. Data* **2004**, *49*, 1639–1642.

(14) Selvi, B.; Patel, S.; Savva, M. Physicochemical characterization and membrane binding properties of camptothecin. *J. Pharm. Sci.* **2008**, *97*, 4379–4390.

(15) Simonelli, A. P.; Mehta, S. C.; Higuchi, W. I. Dissolution rates of high energy polyvinylpyrrolidone (PVP)-sulfathiazole coprecipitates. *J. Pharm. Sci.* **1981**, *70*, 538–549.

(16) Levich, V. G. *Physico-Chemical Hydrodynamics*; Prentice-Hall: NJ, 1962.

(17) Yu, L. X.; Carlin, A. S.; Amidon, G. L.; Hussain, A. S. Feasibility studies of utilizing disk intrinsic dissolution rate to classify drugs. *Int. J. Pharm.* **2004**, *270*, 221–227.

(18) Posokhov, Y. Spectral-luminescent and solvatochromic properties of anticancer drug camptothecin. *J. Photochem. Photobiol. A: Chem.* **2003**, *158*, 13–20.

(19) Strel'tsov, S. A.; Grokhovskii, S. L.; Kudelina, I. A.; Oleinikov, V. A.; Zhuze, A. L. Interaction of topotecan, a DNA topoisomerase inhibitor, with dual-stranded polydeoxyribonucleotides. 1. Dimerization of topotecan in solution. *Mol. Biol.* **2001**, *35*, 432–441.

(20) Jencks, W. P. *Handbook of Biochemistry and Molecular biology*; CRC: OH, 1976.

(21) Raff, L. M. *Principles of Physical Chemistry*; Prentice-Hall: NJ, 2001.

(22) Serajuddin, A. T.; Jarowski, C. I. Effect of diffusion layer pH and solubility on the dissolution rate of pharmaceutical acids and their sodium salts. II: Salicylic acid, theophylline, and benzoic acid. *J. Pharm. Sci.* **1985**, *74*, 148–154.

(23) Mooney, K. G.; Mintun, M. A.; Himmelstein, K. J.; Stella, V. J. Dissolution kinetics of carboxylic acids I: effect of pH under unbuffered conditions. *J. Pharm. Sci.* **1981**, *70*, 13–22.

(24) Murphy, D.; Rodriguez-Cintron, F.; Langevin, B.; Kelly, R. C.; Rodriguez-Hornedo, N. Solution-mediated phase transformation of anhydrous to dihydrate carbamazepine and the effect of lattice disorder. *Int. J. Pharm.* **2002**, *246*, 121–34.

(25) Wang, S. L.; Lin, S. Y.; Hsieh, T. F.; Chan, S. A. Thermal behavior and thermal decarboxylation of 10-hydroxycamptothecin in the solid state. *J. Pharm. Biomed. Anal.* **2007**, *43*, 457–463.

Received for review March 19, 2009. Accepted June 7, 2009.

JE900283V